Real-Time Cross-Correlation Image Analysis of Early Events in IgE Receptor Signaling

Raibatak Das, Stephanie Hammond, David Holowka, and Barbara Baird
Department of Chemistry and Chemical Biology, Cornell University, Ithaca, New York

ABSTRACT Signaling in mast cells and basophils is mediated through IgE and its high affinity cell surface receptor, FcεRI. Crosslinking of the receptors by a cognate multivalent antigen leads to degranulation and release of mediators of the allergic immune response. Using multicolor fluorescence confocal microscopy, we probed the spatio-temporal dynamics of early events in the IgE receptor signal cascade. We monitored the recruitment of GFP-/CFP-labeled signaling proteins by acquiring sequential images with time resolution of 3 s during stimulation of RBL-2H3 mast cells with multivalent antigen. A fluorescent tag on the antigen allowed us to visualize the plasma membrane localization of crosslinked receptors, and fluorescent cholera toxin B served as a plasma membrane marker. We developed an automated image analysis scheme to quantify the recruitment of fluorescent intracellular proteins to the plasma membrane and to assess the time-dependent colocalization of these and other membrane-associated proteins with crosslinked receptors as measured by cross-correlation between the plasma membrane distributions of the two fluorophores. This automated method permits analysis of thousands of individual images from multiple experiments for each cross-correlation pair. We systematically applied this analysis to characterize stimulated interactions of IgE receptors with several signaling proteins, including the tyrosine kinases Lyn and Syk, and the adaptor protein LAT. Notably, for Syk-CFP we observed a rapid stimulated translocation to the plasma membrane but very little colocalization with aggregated receptors. Our results demonstrate the utility of this simple, automated method to monitor protein interactions quantitatively during cell signaling.

INTRODUCTION

Mast cells and basophils are hematopoietic cells of the myeloid lineage and the primary effectors of Type I hypersensitivity, i.e., the allergic immune response (1). These cells express on their surface the high affinity IgE receptor, FcεRI, and they bear numerous cytoplasmic granules rich in preformed vasoactive mediators such as histamine. Crosslinking of IgE bound to FcεRI by a cognate multivalent antigen initiates a signal cascade resulting in degranulation and mediator release (2). FcεRI is a prototype of the family of multichain immune recognition receptors whose other members include the T-cell receptor and B-cell receptor. FcεRI on mast cells consists of an α-subunit containing an extracellular IgE binding domain, a β-subunit, and two disulfide-linked γ-subunits containing immunoreceptor tyrosine-based activation motifs (ITAMs) that are critical for signal transduction (2). Receptor crosslinking results in phosphorylation of the β- and γ-subunits at their ITAM sequences by the membrane-associated protein tyrosine kinase, Lyn. Phosphorylated ITAMs on the γ-subunit bind tandem Src-homology 2 (SH2) domains on the tyrosine kinase, Syk, which is activated through a conformational change and tyrosine phosphorylation (3,4). Activated Syk phosphorylates several downstream targets, among them the adaptor protein linker for activation of T cells (LAT), and phospholipase Cγ. These proteins activate several different pathways that lead to production of lipid second messengers, Ca^{2+} mobilization, and ultimately degranulation (2).

These cell-signaling events require interactions among multiple components, and such interactions have been detected biochemically, by immunoprecipitation experiments, and observed by microscopic imaging of labeled signaling proteins. Confocal fluorescence microscopy is a valuable tool for direct visualization of signaling proteins in fixed or living cells. Using genetically encoded fluorescent proteins as probes in live cells, confocal fluorescence microscopy can be used to reveal the subcellular localization and dynamics of selected intracellular proteins on the micron scale (5). This direct visualization permits precise quantification of spatial colocalization between signaling components and crosslinked receptor complexes. Such quantification is relevant for monitoring events mediated by both protein-protein and protein-lipid interactions, including those involving membrane domains known as lipid rafts (6).

Individual confocal images were previously used to quantify the cross-correlation between plasma membrane distributions of fluorescent receptor complexes and labeled signaling proteins, as a measure of their relative colocalization, after significant receptor patching had occurred (7,8). In this study, we describe a set of image analysis tools that facilitate the automation of these measurements, thereby enabling rapid analysis of hundreds of sequential images acquired using real-time multicolor confocal imaging. We applied this image analysis scheme to quantify the time course of plasma membrane recruitment and colocalization with crosslinked IgE receptors of several different functional

Submitted January 30, 2007, and accepted for publication January 28, 2008.

Address reprint requests to Barbara Baird, Tel.: 607-255-4095; E-mail: bab13@cornell.edu.

Raibatak Das's present address is Dept. of Mathematics, University of British Columbia, Vancouver, BC, Canada.

Editor: Petra Schwille.

0006-3495/08/06/4996/13 $2.00

doi: 10.1529/biophysj.107.105502

subdomains and holoproteins involved in the FcεRI signaling pathway. Our analysis reveals plasma membrane translocation and receptor colocalization dynamics with high temporal resolution, and demonstrates the general utility of this approach for the study of signaling processes in live cells.

MATERIALS AND METHODS

Materials

Monoclonal anti-2,4-dinitrophenyl (DNP) IgE (9) was purified as previously described (10). Alexa 488 and Alexa 546 labeling kits from Invitrogen (Carlsbad, CA) were used for labeling anti-DNP IgE as previously described (11). Alexa 555-cholera toxin subunit B (A555-CTB) was purchased from Invitrogen. Cy5 from Amersham Pharmacia (Buckinghamshire, England) and Alexa 647 from Invitrogen were used for labeling DNP-BSA in pH 8.5 borate-buffered saline: 200 mM boric acid, 33 mM NaOH, and 160 mM NaCl. Dye and protein in the recommended ratio were incubated overnight in the dark at room temperature. The reaction mixture was extensively dialyzed against pH 7.4 phosphate-buffered saline (PBS)-EDTA to remove unbound dye. cDNA constructs of GFP-(PLC-γ1)-$(SH2)_2$ (7) and Syk-CFP (ATCC id: 10373748) were gifts from Dr. Tobias Meyer (Stanford University); GFP-protein kinase B (Akt)-pleckstrin homology (PH) (12) was from Dr. Kenneth Field (Bucknell University); LAT-EGFP (13) was from Dr. Lawrence Samelson (National Institutes of Health); ECFP-InsP51 (14) and DsRed N1-PLCδ PH were from Dr. Andreas Jeromin (Allen Institute for Brain Science, Seattle, WA); GFP-Cdc42-N17 (15) was from Dr. Jon Erickson (Cornell University). Polyclonal rabbit anti-Syk (N-19) was from Santa Cruz Biotechnology (Santa Cruz, CA), and Alexa 555 goat anti-rabbit IgG was from Invitrogen.

Cell culture and transfection

RBL-2H3 cells (16) are a subline of rat basophilic (RBL) cells that were maintained in monolayer culture and harvested as previously described (17). The cells were plated overnight in 35 mm MatTek dishes (MatTek, Ashland, MA) at a subconfluent density ($\sim 4 \times 10^5$ cells per dish) before transfection. Lipofectamine 2000 was used to transiently transfect the cells with GFP or CFP conjugates of specific signaling proteins, as previously described (11), or cells stably expressing PM-EGFP were used (8). Posttransfection, the cells were sensitized overnight with 1 μg/ml unlabeled anti-DNP mouse IgE and used the next day for microscopy. For one set of experiments, the cells were sensitized for 30 min at room temperature with 5 μg/ml Alexa 546-labeled anti-DNP IgE. Before imaging, the cells were washed and incubated in 1 ml of a buffered saline solution (20 mM HEPES, 135 mM NaCl, 5 mM KCl, 1.8 mM $CaCl_2$, 1 mM $MgCl_2$, 5.6 mM glucose, and 1 mg/ml BSA, adjusted to pH 7.4), and incubated at 37°C. Immediately before image acquisition the cells were labeled for 2 min at room temperature ($\sim$22°C) with 200 μl of 2 μg/ml A555-CTB. The cells were washed with excess buffer to remove unbound label, and 2.5 ml buffered saline solution at 37°C was added.

Immunocytochemical labeling

RBL-2H3 cells were plated overnight in MatTek wells, sensitized for 2 h with Alexa488-IgE, then stimulated with DNP-BSA for indicated times at 37°C and fixed with 4% (w/v) paraformaldehyde in PBS, pH 7.2, for 20 min at room temperature. Fixed cells were labeled in PBS/0.01% sodium azide with 1% BSA and 0.01% saponin using rabbit anti-Syk (N-19; 1/50dil), followed by Alexa 555-goat anti-rabbit IgG (10 μg/ml), each for 1 h, with wash steps after each incubation.

Confocal fluorescence imaging of living cells

Confocal images were acquired on a Leica TCS SP2 laser scanning confocal system (Leica Microsystems, Exton, PA) using an upright microscope with a 63× 0.9 numerical aperture HCX APO L U-V-I water immersion objective (Leica 506148). The system is equipped with a four-line Ar laser, two HeNe lasers, and an acousto-optical tunable filter to control the laser intensities. The microscope stage was enclosed by a chamber heated through a feedback temperature control to maintain the buffer in the MatTek dish at 35–37°C. The excitation laser wavelengths and the range of emission wavelengths for the various fluorophores were as follows: CFP, $\lambda_{ex} = 458$ nm, $\lambda_{em} = 465$–550 nm; GFP and Alexa 488, $\lambda_{ex} = 488$ nm, $\lambda_{em} = 500$–550 nm; Alexa 555, $\lambda_{ex} = 543$ nm, $\lambda_{em} = 560$–630 nm; Cy5 and Alexa 647, $\lambda_{ex} = 633$ nm, $\lambda_{em} = 640$–750 nm. For experiments with Alexa 546 IgE, fluorescence was excited at $\lambda_{ex} = 543$ nm and emission was collected over 560–700 nm. For each experiment with a particular GFP- or CFP-labeled protein, a field of view containing 1–3 transfected cells was chosen and maintained throughout the experiment. Fields of view were carefully chosen to ensure that no other cells abutted the transfected cells, as ascertained by examining the A555-CTB label. A subconfluent density of cells usually yields several such fields in a dish.

To quantify the time-dependent recruitment of cytosolic probes to the plasma membrane (PM), and the association of signaling proteins with crosslinked FcεRI, we imaged an equatorial confocal section of the transfected cells, typically once every 3 s. A laser scan rate of 800 Hz was used, with two successive line scans averaged together. Small manual focusing corrections were applied periodically during the experiment to compensate for minor stage drifts in the vertical direction. Images were collected for 3 min (3 s/frame × 61 frames) before antigen addition. A 0.5-ml aliquot of the antigen, 6 μg/ml of Cy5-DNP-BSA (or A647-DNP-BSA), was added to the dish and rapidly mixed to a final concentration of 1 μg/ml, and the image acquisition was resumed within 10–20 s after antigen addition. The same cells that were imaged before antigen addition were then imaged every 3 s for an additional 20 min (401 frames).

We use the following nomenclature to describe the various fluorophores, unless otherwise noted. (C/G)FP conjugated endogenous proteins and Alexa 488-IgE are all referred to as the green label, Alexa 555-CTB or Alexa 546-IgE as the membrane label, and Cy5-DNP-BSA or A647-DNP-BSA as the red label. Therefore, in the preantigen image stack, each ''frame'' consisted of two images, one in the green channel and one in the membrane channel; and in the post antigen stack, three images, one each in the green channel, the membrane channel, and the red channel, comprised each frame. All images were saved as 12-bit grayscale Tif format files. To minimize bleedthrough from the green-label signal into the membrane channel, we collected images in a sequential acquisition mode. Before antigen addition, the green channel and the membrane channel were scanned alternately. After antigen addition, the green and red channels were simultaneously scanned and the membrane channel was scanned alone in an alternating sequence. In the absence of any Cy5, or in the presence of Cy5 without any excitation from the 633-nm laser, there was no detectable signal above the background due to bleedthrough into the red channel.

Image analysis

ImageJ (http://rsb.info.nih.gov/ij/) and MatLab (The MathWorks, Natick, MA) were used for postacquisition image analysis (computer code available upon request). For each cell to be analyzed in an experiment, two polygonal regions of interest (ROIs) were selected in ImageJ, one for the preantigen image stack and one for the postantigen image stack. The ROIs were chosen to enclose the selected cell and eliminate any others for the entire image stack. The coordinates of these enclosing polygons were noted and then used as inputs in the MatLab scripts that carry out the remainder of the image analysis. The image analysis consisted of three main tasks:

1. Using the membrane label image to extract a binary mask defining the PM.
2. Using this binary PM mask determine the mean intensity of the green label at the PM.
3. Calculating the cross-covariance between the PM distribution of the green and the red labels to quantify the colocalization between the two labels at the PM.

The details of each task are described below. For each frame of the preantigen stack (typically 61 frames) we determined the PM mask and the mean intensity of the green channel at the PM. For each frame of the postantigen stack (typically 401 frames) we determined, in addition, the cross-covariance between the green and red channel PM intensity distributions. Further, we systematically corrected the postantigen green channel PM intensity to compensate for loss of overall intensity due to photobleaching.

Task 1

To extract a binary PM mask from the original image of the membrane channel, we first applied a threshold to convert the 12-bit intensity image to a binary image. The threshold intensity was determined using the Otsu algorithm that minimizes intraclass variance (18). The built-in MatLab ''graythresh'' function that calculates the threshold for an 8-bit or 16-bit image using the Otsu algorithm was modified for use with 12-bit images. The cell under consideration was then selected in this thresholded binary image using the polygonal ROI generated previously, and a median filter applied to the resulting image to eliminate a majority of the shot-noise. To enhance the connectivity of the PM segments, and further reduce contributions from extraneous pixels and small structures that are not a part of the plasma membrane, we applied a morphological closing operation with a disk of one-pixel radius, followed by a morphological opening operation with a disk of two-pixel radius, respectively, as the structuring elements. The structuring element matrices were used as defined in MatLab. The resultant binary image after these operations was deemed to be the binary PM mask for the cell of interest—with the ''on'' pixels (those with value 1) defining the PM and the ''off'' pixels (value 0) constituting the rest of the image, including the cytosol, extracellular areas, and all the other cells in the field. The successive steps of the image segmentation process described above are illustrated for a sample membrane channel image in Fig. 1. Typically, the mask is an annular ring with thickness that varies between 5 and 10 pixels, barring occasional missing spots. This PM mask was then used for calculating the average PM intensity in the green channel and the cross-covariance between the PM distributions of the green channel and red channel intensities.

Task 2

The average PM intensity in the green channel was calculated as the mean of the individual pixel intensities in the green channel for all pixels that are part of the PM. Formally, this mean intensity, $\bar{G}_{\mathrm{PM}}$, is defined as

$$\bar{G}_{\mathrm{PM}} = (1/n)\sum_{\mathrm{i}=1}^{\mathrm{n}} G_{\mathrm{i}}, \tag{1}$$

where G_{i} is the green channel intensity of the i^{th} ''on'' pixel in the PM mask, with a total n ''on'' pixels in the PM mask.

To account for changes in the overall intensity of the fluorophore due to photobleaching and any instrumental drift, we also calculated the whole-cell green channel intensity for each cell in the postantigen stack. The whole cell intensity was defined to be the sum of green channel intensities of all pixels in the ROI enclosing that cell. Using the first image of the postantigen stack as a baseline, we then calculated a multiplicative correction factor to compensate for changes in the overall intensity, defined as

$$f = 1 + (G^0_{\mathrm{tot}} - G_{\mathrm{tot}})/G^0_{\mathrm{tot}}, \tag{2}$$

where G_{tot} is the whole-cell green channel intensity of the frame under consideration, and G^0_{tot} is the whole-cell green channel intensity of the first frame in the postantigen stack. The average PM intensity was multiplied by this correction factor, such that $(\bar{G}_{\mathrm{PM}})_{\mathrm{corr}} = f\bar{G}_{\mathrm{PM}}$ is the corrected average PM intensity in the green channel.

Task 3

To calculate the cross-covariance between the PM intensity distributions of the green and the red channels, we first determined the coordinates, $(\bar{x}, \bar{y})$, of the PM mask intensity centroid, that are defined as

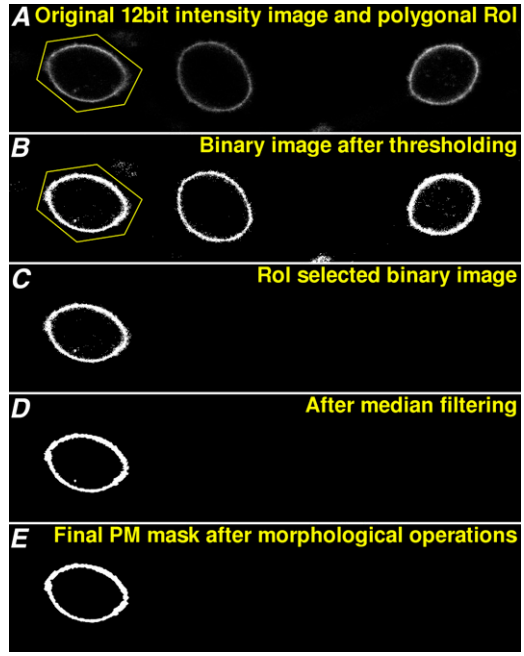

FIGURE 1 Image segmentation to transform a membrane channel image to a binary PM mask. A series of image processing operations transform a 12-bit intensity image of a PM label (most frequently, A555-CTB) to a binary PM mask for a single cell. (*A*) The original membrane channel image is a 12-bit grayscale intensity image. The outline of a polygonal ROI that was chosen to enclose the cell of interest is shown in yellow. (*B*) The grayscale image is thresholded to convert it to a binary image, and (*C*) the polygonal ROI is applied to select-out the cell of interest. (*D*) Median filtering of the thresholded image removes a majority of the speckled shot-noise. (*E*) A morphological closing followed by a morphological opening eliminate further nonconnected pixels—such as those resulting from internalized vesicles, shown in *D*—and result in the final binary PM mask.

$$\bar{x} = \frac{\sum_{\mathrm{j}=1}^{\mathrm{m}}(x_{\mathrm{j}} \times I_{\mathrm{j}})}{\sum_{\mathrm{j}=1}^{\mathrm{m}} I_{\mathrm{j}}}, \quad \bar{y} = \frac{\sum_{\mathrm{j}=1}^{\mathrm{m}}(y_{\mathrm{j}} \times I_{\mathrm{j}})}{\sum_{\mathrm{j}=1}^{\mathrm{m}} I_{\mathrm{j}}}, \tag{3}$$

where m is the total number of pixels (''on'' + ''off'') in the PM mask and I_{j} is the intensity of a given pixel whose coordinates are $(x_{\mathrm{j}}, y_{\mathrm{j}})$. Each image is represented in MatLab as a two-dimensional matrix, and x_{j} and y_{j} are the column and row indices, respectively, of the j^{th} pixel. The quantity m = (number of rows) × (number of columns) of the image matrix. For a binary image,

$$I_{\mathrm{j}} = \begin{cases} 1 & \text{if the } j^{\mathrm{th}} \text{ pixel is on,} \\ 0 & \text{if the } j^{\mathrm{th}} \text{ pixel is off,} \end{cases} \tag{4}$$

and therefore, it is evident that for the binary PM mask the coordinates of the intensity centroid are the mean x and y coordinates of all the ''on'' pixels. With this intensity centroid as the origin of a new coordinate system, each ''on'' pixel at the location $(x_{\mathrm{k}}, y_{\mathrm{k}})$ $1 \le k \le n$ (n = the total number of ''on'' pixels) in the image coordinates was next assigned an angle

$$\theta_{\mathrm{k}} = \arctan\left(\frac{\bar{y} - y_{\mathrm{k}}}{x_{\mathrm{k}} - \bar{x}}\right) \tag{5}$$

in the intensity centroid coordinates, chosen to lie in the range $-\pi \le \theta_{\mathrm{k}} \le \pi$, as schematically illustrated in Fig. 2. With this definition, θ_{k} is the angle about the x axis in a standard right-handed Cartesian coordinate system with the origin at the intensity centroid and the positive x axis extending along the increasing column number of the image matrix.

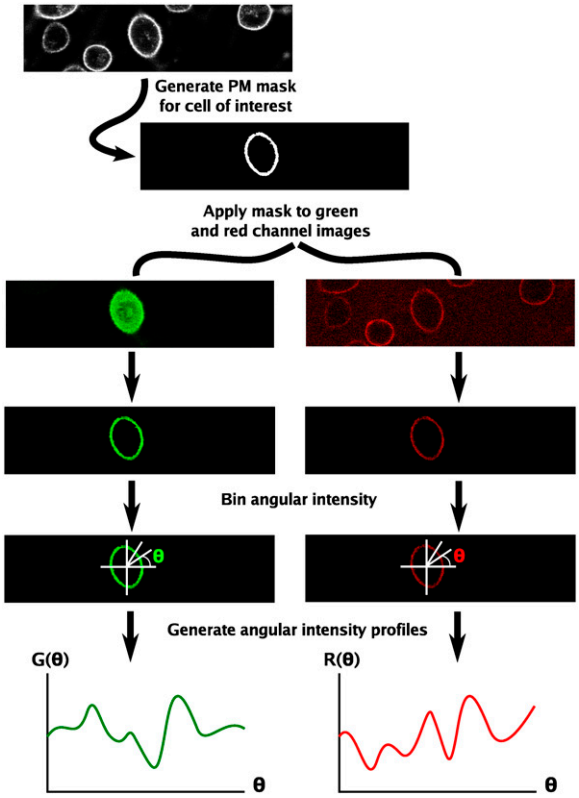

FIGURE 2 A schematic illustration of the angular intensity profile assignment to the green and red channel images using the PM mask to extract the PM distribution of the two fluorophores, followed by binning of all the PM pixels into discreet angular segments to determine the angular intensity profile.

Next, we binned all the ''on'' PM pixels into 90 equally spaced angular intervals between $-\pi$ and π (each such interval spans a 4° angle) and calculated the mean intensity in the green and the red channels of all the pixels in each angular interval. This binning gives two angular intensity distributions $G(\theta_i)$ and $R(\theta_i)$, respectively, for the green and the red channels, where θ_i assumes 90 uniformly spaced, discreet values between $-\pi$ and π, i.e., $\theta_i = i\pi/45$; $i = -45, -44, \ldots, 0, \ldots 44$. The normalized peak cross-covariance between these two angular intensity distributions, also known as Pearson's correlation coefficient (19), is defined as

$$\rho_0 = \frac{\sum_i [(G(\theta_i) - \bar{G}) \times (R(\theta_i) - \bar{R})]}{\left[\sum_i (G(\theta_i) - \bar{G})^2\right]^{1/2} \times \left[\sum_i (R(\theta_i) - \bar{R})^2\right]^{1/2}}, \quad (6)$$

and was calculated for each frame of the postantigen image stack.

RESULTS AND DISCUSSION

An automated image analysis scheme to quantify PM recruitment and receptor colocalization

We imaged living RBL-2H3 mast cells expressing a variety of (C/G)FP labeled holoproteins and functional protein subdomains at physiologically relevant temperatures (35–37°C) and with a high temporal resolution of 3 s/frame. The cells were sensitized with anti-DNP IgE; then a fluorescent antigen, Cy5-DNP-BSA (or A647-DNP-BSA), was used to crosslink the IgE and visualize receptor aggregation on the surface of these cells. Our image analysis scheme quantified the relative overlap between the intensity distribution in the green channel (fluorescent protein conjugate) image and the red channel (antigen) image at the plasma membrane (PM).

To visualize the PM, we perform a short, 2 min incubation with A555-CTB at room temperature immediately before image acquisition. CTB pentavalently binds the ganglioside GM_1 with a high affinity and other gangliosides to a lesser extent (20), and it effectively labels the entire PM. Under these conditions, A555-CTB is visible as an optically uniform PM label (Fig. 1 *A*). Studies in our laboratory have shown that CTB binding to PM does not detectably alter the signaling via FcεRI in RBL-2H3 cells, as measured by stimulated Ca^{2+} mobilization (unpublished data).

The first part of our image analysis scheme consists of an image segmentation algorithm that uses the CTB image from each time point to construct a binary mask delineating the PM of the cell at that time point. The transformation of the original image to this binary mask is illustrated in Fig. 1, where a typical CTB image (Fig. 1 *A*) undergoes a series of operations that include thresholding (Fig. 1 *B*), median filtering (Fig. 1 *D*), and morphological closing and opening that results in the binary PM mask (Fig. 1 *E*) for a selected cell in the original field of view. Also shown in the first two panels of Fig. 1 is a polygonal region of interest (ROI) chosen to circumscribe the cell of interest and isolate it from all other cells in that field of view. Selecting such an ROI minimizes the contribution from any extracellular objects in the field of view. The image segmentation algorithm further eliminates contributions from any small intracellular vesicles that arise from membrane trafficking.

Fig. 3 illustrates the evolution of the A555-CTB label (*left panel*) and the corresponding PM masks (*center panel*) during a typical experiment. The A555-CTB label becomes slightly more heterogeneous during the course of the experiment, but this heterogeneity is less pronounced than what is observed for the PM distribution of the antigen under these conditions (Cy5-DNP-BSA images in the *right panel* of Fig. 3 and *center panel* of images in Fig. 4 *A*). Importantly, small-scale heterogeneities of the CTB label have little effect on the image segmentation algorithm, and, as seen in Fig. 3 (*center panel*), the algorithm effectively isolates a membrane mask of nearly uniform thickness along the periphery of a cell. Some small internalized vesicles labeled with A555-CTB are evident in the grayscale images, and the segmentation algorithm effectively eliminates these while retaining the PM label to define the PM mask.

The binary PM mask generated by the segmentation algorithm allows us to measure the degree of translocation of cytosolic signaling components and their relative overlap with crosslinked receptor in a straightforward fashion. Any pixel in the binary PM mask can only assume two values: 1 or ''on,'' when a pixel is determined to lie on the PM, and 0 or ''off'' otherwise. Therefore applying this mask on the green

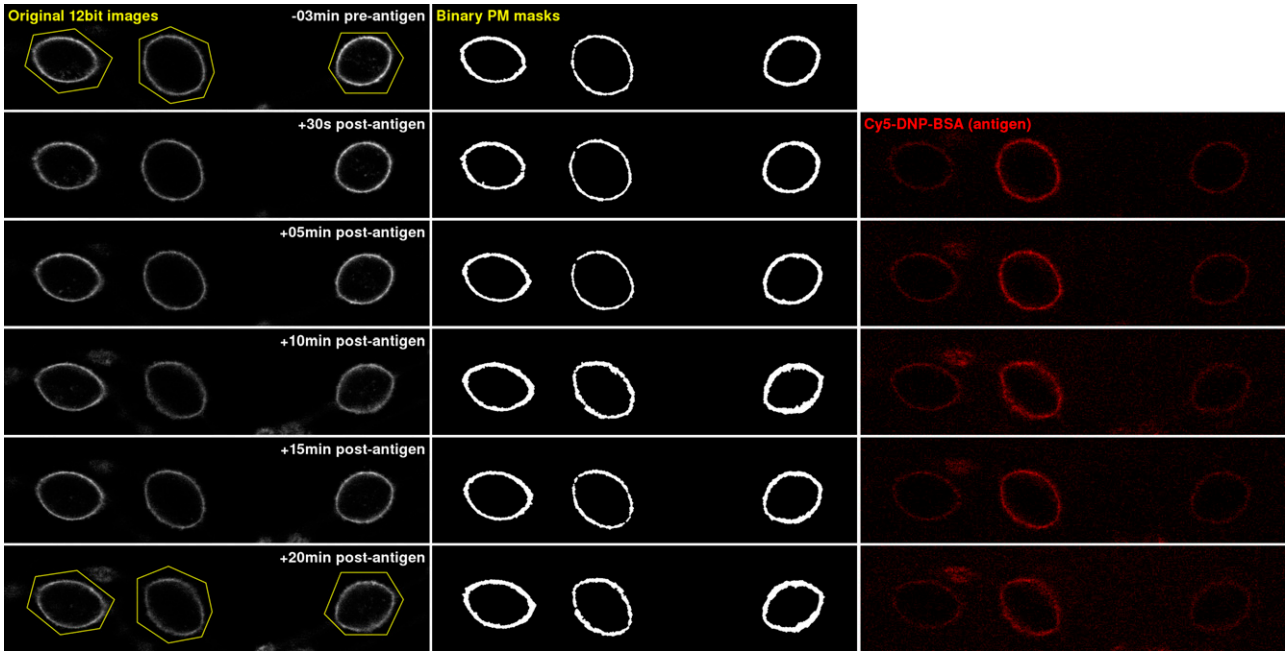

FIGURE 3 Representative samples of A555-CTB images acquired from a single experiment and the resulting automatically generated binary PM masks. The left panel shows the original images and the center panel, the combined PM masks for three cells in the field of view. The right panel shows the antigen label images for the corresponding time points after antigen addition. Also shown are the outlines of the preantigen (*top left*) and postantigen (*bottom left*) ROIs used to demarcate the three cells.

and the red channel images to extract the PM distribution for the two other fluorophores simply consists of an element-by-element multiplication of all the pixels in the green or the red channel image with the corresponding pixels of the PM mask, such that only the pixels that are ''on'' in the binary mask retain their original intensity value, and all the other pixels that are ''off'' in the mask are now set to have 0 intensity. We averaged the intensity values of all the green channel pixels that are ''on'' in the PM mask and used this average intensity (Eq. 1) as a measure of the relative amount of the green fluorophore at the PM.

The colocalization between the PM distributions in the red and the green channels is quantified by the cross-covariance peak between the two PM distributions. As schematically illustrated in Fig. 2, to calculate the cross-covariance we assign a discrete angular intensity profile to the PM distributions in the two channels. All ''on'' PM mask pixels are binned into 90 equally spaced angular segments spanning a 4° angle each, with the angle defined about the intensity centroid. The intensities of all the pixels in each angular segment are averaged, and the averaged values define the angular intensity profiles $G(\theta_i)$ and $R(\theta_i)$ for the green and the red channels, respectively. These angular intensity profiles are calculated for each cell under consideration in every frame of the image stack. We adopted this angular representation of the intensity profile as an alternative to the more usual linear intensity profile generated from a line trace of the PM because it is better suited to take into account the finite thickness of the PM mask. The binning was chosen to ensure that any instrumental artifacts that arise out of suboptical pixilation are averaged out. RBL cells are typically $\sim$10 μm in diameter, and a 4° arc is therefore 10 μm $\times$ 4π /360 $\approx$ 350 nm long, which well exceeds the $\sim$200 nm limit of resolution for confocal microscopy. The peak cross-covariance value ρ_0 between the two angular intensity profiles, as defined in Eq. 6, was calculated at each time point for a given cell and used to quantify the relative overlap between the red and the green fluorophores at the PM.

Initial evaluation: PM recruitment of PLCγ-(SH2)$_2$ and its colocalization with the IgE receptor

We tested the general applicability of our method by examining the translocation from cytosol and the colocalization with crosslinked receptor of the GFP-conjugated tandem SH2 domain of phospholipase C-γ1 (GFP-(PLCγ1)-(SH2)$_2$). This fluorescently-labeled functional domain was previously characterized in RBL-2H3 cells by Stauffer and Meyer (7) who demonstrated that upon antigen crosslinking it rapidly translocated from a uniform cytosolic distribution to a punctate PM distribution. We observe a similar redistribution of this probe to the PM and a significant increase in colocalization with the crosslinked IgE receptor. Fig. 4 *A* shows confocal equatorial images of selected time points for a representative experiment in which this translocation of GFP-(PLCγ1)-(SH2)$_2$ to the plasma membrane is evident in two transfected cells after addition of Cy5-DNP-BSA. Quantified time courses of PM association for these two cells are shown

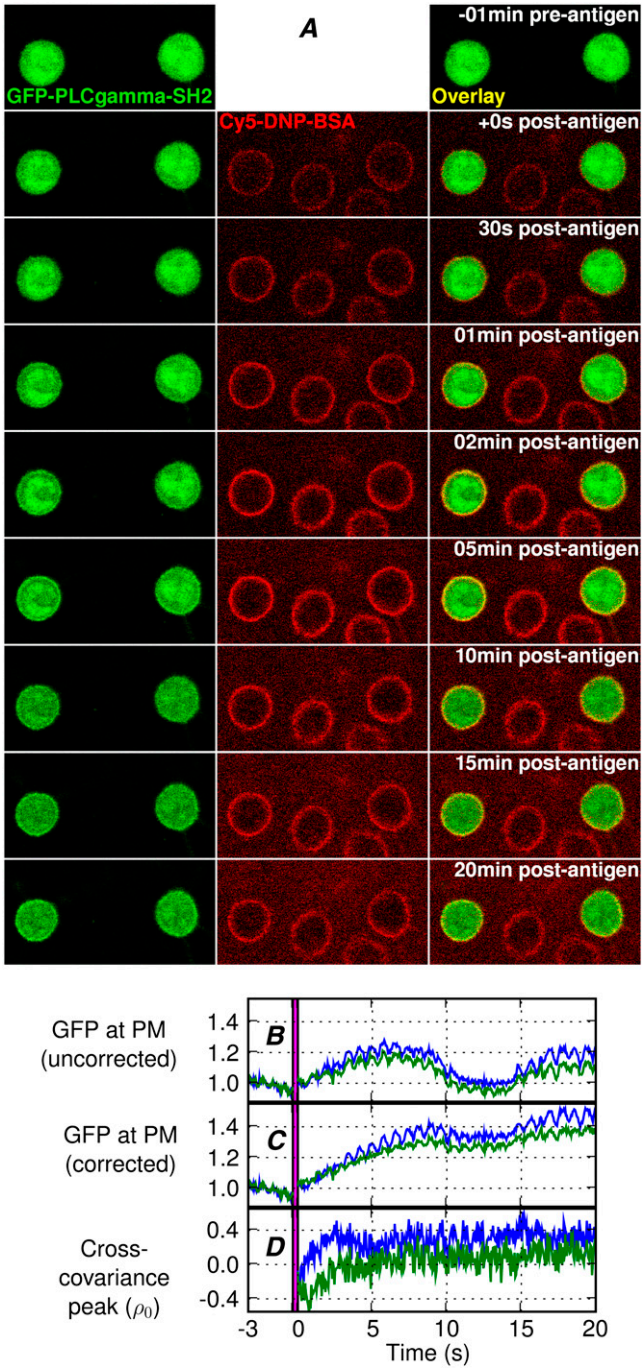

FIGURE 4 The dynamics of GFP-(PLC-γ1)-$(SH2)_2$ distribution before and after receptor crosslinking. (*A*) Images from a representative experiment show the translocation of GFP-(PLC-γ1)-$(SH2)_2$ from a relatively uniform and predominantly intracellular distribution to a punctate plasma membrane distribution that colocalizes with the IgE receptor. Left panels show the green channel images (GFP), center panels show the red channel images (antigen), and right panels show the overlayed images before and at various time points after antigen addition. (*B* and *C*) The mean intensity in the green channel at the PM for the two transfected cells in *A* (blue and green traces), calculated using the image analysis scheme described in Materials and Methods, before (*B*) and after (*C*) applying the photobleaching correction derived from changes in whole-cell intensity. The intensity values shown are normalized with respect to the average of the intensity values before antigen addition (i.e., the average of the first 61 frames). The vertical bar at $t = 0$ in this and the following figures indicates the time of antigen addition before resuming image acquisition. (*D*) The colocalization of the GFP-(PLC-γ1)-$(SH2)_2$ with IgE receptors quantified by the peak cross-covariance values (ρ_0, Eq. 6) for the PM intensity distributions of the red and green channels for the two transfected cells shown in *A*.

before (Fig. 4 *B*) and after correction for time-dependent photobleaching (Fig. 4 *C*), using changes in total cellular fluorescence at each time point for this correction (Eq. 2). These two cells exhibit evidence for a slow biphasic recruitment of GFP-(PLCγ1)-$(SH2)_2$ to the PM over the 20-min time course of measurement, and this biphasic recruitment is also evident in the average time course of multiple cells (see Fig. 6 *A*). The higher frequency oscillations evident in Fig. 4, *B* and *C*, are caused by instrumental vibrations that disappear in averages of multiple cells. A closer visual examination of the confocal images in Fig. 4 *A* indicates that the bright pool of GFP-(PLCγ1)-$(SH2)_2$ in the nucleus that is evident in early time points is substantially diminished after 5 min of stimulation. Redistribution of this nuclear pool may be related to the second phase of PM accumulation that is evident after 10 min in Fig. 4 *C* and 6 *A*.

The time course of colocalization of GFP-(PLCγ1)-$(SH2)_2$ with crosslinked receptors, as measured by the peak cross-covariance (ρ_0) between the PM distribution of antigen and the EGFP label is shown for these two cells in Fig. 4 *D*, and the average time course for multiple cells from eight separate experiments is shown in Fig. 5 *A*. These data show a time-dependent increase in ρ_0 during the first 300 s and a relatively constant value for at least 15 min thereafter. This time course represents an average increase from $\rho_0 \sim 0$ just after antigen addition to $\rho_0 \sim 0.2$ at its maximal value, indicating a modest degree of colocalization of GFP-(PLCγ1)-$(SH2)_2$ with crosslinked FcϵRI. Shown in Supplementary Material, Data S1, Fig. S1 are several examples of cells with visibly evident colocalization of antigen and GFP-(PLCγ1)-$(SH2)_2$, and corresponding ρ_0 values that are somewhat larger than this average.

In their analysis, Stauffer and Meyer (7) used CTB as a marker of glycosphingolipid-enriched membrane domains, and they observed strong overlap of GFP-(PLCγ1)-$(SH2)_2$ with membrane punctae of CTB after receptor crosslinking. As indicated above, CTB is mostly uniform at the PM in our cells, but, as shown in Fig. 5 *B*, we observe a time-dependent increase in ρ_0 between CTB and GFP-(PLCγ1)-$(SH2)_2$ after addition of antigen that is consistent with their observations. This time course is similar to that for GFP-(PLCγ1)-$(SH2)_2$ and antigen during the first 300 s, but deviates from this at longer time periods (Fig. 5, *A* and *B*), indicating some differences in the spatio-temporal relationships of these PM components during cell stimulation. A possible explanation for the similar initial time course and magnitude of GFP-(PLCγ1)-$(SH2)_2$ cross-correlation with antigen and CTB is the colocalization of these components in glycosphingolipid-enriched membrane domains, commonly called ''lipid rafts'' (21).

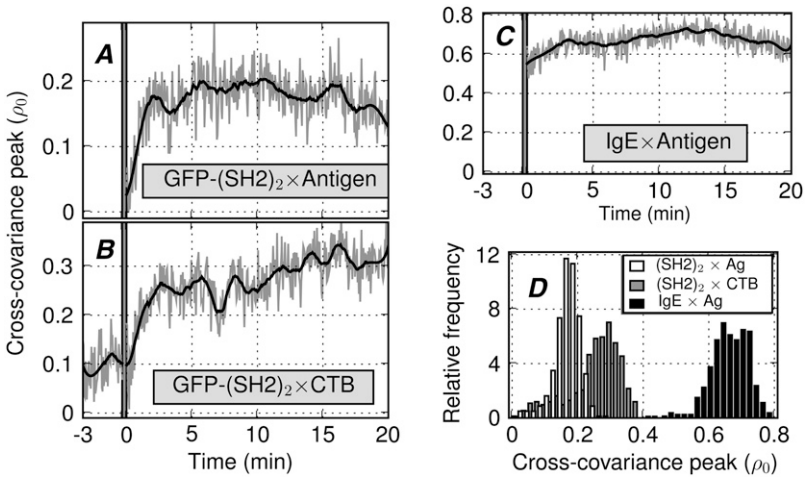

FIGURE 5 Colocalization dynamics of GFP-(PLC-γ1)-$(SH2)_2$ with (*A*) crosslinked IgE receptor and (*B*) CTB, as measured by the peak cross-covariance (ρ_0) between their PM distributions. The ρ_0 value shown at each time point is the average of data for 8–16 cells from 4–8 independent experiments on different days. For the plot in *B*, the angular intensity profile of the A555-CTB label was determined from the membrane channel images using the same angular binning scheme used for extracting the angular intensity profiles of the green and red channels. Since the membrane label is present before antigen addition, we could calculate the pre-antigen cross-covariance between the CTB and the GFP labels, plotted here. (*C*) Colocalization dynamics of multivalent antigen with IgE receptor as measured by peak cross-covariance between Cy5-DNP-BSA and A488 anti-DNP IgE. (*D*) The distribution of peak cross-covariance values between various fluorophore pairs with values from all time points included in the histograms shown. The relatively wide shoulder for the cross-covariance between GFP-(PLC-γ1)-$(SH2)_2$ and A555-CTB is due to the low cross-covariance values before antigen addition. The smooth lines through the cross-covariance data for *A–C* and in subsequent figures were generated using a Savitzky-Golay smoothing filter (44), and are shown here to indicate overall trend of the data.

To test whether the nanoscale localization of CTB to lipid-raft domains might affect its use to delineate the micron-scale PM mask in our studies, we carried out cross-correlation analysis between GFP-(PLCγ1)-$(SH2)_2$ and antigen using an alternate PM marker, the PIP2-specific PH domain from PLCδ, which Stauffer and Meyer used as a uniform, nonraft PM label in their studies (7). As shown in Data S1, Fig. S2 (*top* and *middle panels*), we found that the use of this PM marker yielded a time-dependent increase in ρ_0 that follows the time course for GFP-(PLCγ1)-$(SH2)_2$ association with the PM in these experiments, with a net increase in ρ_0 after 10 min that is a little larger than that obtained with CTB as the PM mask. These results indicate that the time-dependent colocalization of GFP-(PLCγ1)-$(SH2)_2$ with antigen that is detected by our cross-correlation analysis is not dependent on the PM mask that is used. In these experiments with the nonraft PM label, we also analyzed the cross-covariance between the PM label and antigen, and we observed very limited time-dependent changes in ρ_0 between these two labels (Data S1, Fig. S2, *bottom panel*). Somewhat higher values of ρ_0 are observed for this pair, compared to those between GFP-(PLCγ1)-$(SH2)_2$ and antigen. These relatively higher ρ_0 values are consistent with our observations of cross-covariance between two membrane-associated probes, as further discussed in a following section. Importantly, the lack of a time-dependent increase in ρ_0 indicates that there is no significant redistribution of this nonraft PM label with lipid-raft-associated crosslinked IgE receptors.

In the previous analysis, Pyenta et al. (8) classified a ρ_0 in the range 0.4–1 as a good indicator of coaggregation between two species, with 1 being the theoretical upper limit for two perfectly overlapping signals. The overall changes in ρ_0 and the maximal observed values in our experiments (for example, Fig. 5, *A* and *B*) are modest in comparison, and point to major differences in the experimental conditions used. That study used a 30-min incubation with a primary antibody to label FcεRI and other outer leaflet PM markers, followed by incubation at 4°C with and without secondary crosslinking for several hours. These conditions, particularly with the secondary crosslinking, resulted in large-scale aggregation of crosslinked species and correspondingly high ρ_0 values. By analyzing data from that previous study with our current method, we verified that both methods of cross-correlation analysis give comparable ρ_0 values when applied to the same images (data not shown). The ρ_0 values in our experiments, carried out in real-time at physiological temperatures, are limited by the size and intensity of the much smaller PM punctae, such as those seen in the confocal images in Fig. 4 *A*. Furthermore, the fast laser scan rates used in our experiments also attenuate the signal/noise ratio in our images. To determine a useful upper limit of ρ_0 that is observable under the conditions in our experiments, we measured ρ_0 for A488 anti-DNP IgE and Cy5-DNP-BSA, which are bound to each other and almost completely overlap. As seen in Fig. 5 *F*, ρ_0 between these two species varies between 0.6 and 0.7. Correspondingly, we observe smaller values of ρ_0 for GFP-(PLC-γ1)-$(SH2)_2$ and crosslinked receptor with less pronounced overlap compared to that between the antigen-receptor pair. The histogram in Fig. 5 *G* displays the distribution of calculated ρ_0 values between A488-IgE and Cy5-DNP-BSA and that of GFP-(PLC-γ1)-$(SH2)_2$ with crosslinked receptor and with CTB.

Recruitment and colocalization dynamics of additional cytosolic proteins

In addition to GFP-(PLC-γ1)-$(SH2)_2$, we examined the PM recruitment and receptor colocalization of two other signaling components that are usually cytosolic in unstimulated cells—a GFP-tagged PH domain from Akt (GFP-(Akt)-PH) (22), and carboxy-terminal CFP-tagged tyrosine kinase Syk (Syk-CFP). The time course of antigen-induced PM trans-

location for these probes are plotted in the upper panels of Fig. 6, *A–C*. The lower panels show the time courses of cross-covariance between these probes and antigen, and ρ_0 between the probes and CTB, before and after antigen addition. We observe that GFP-(Akt)-PH exhibits some constitutive PM association in these cells and relatively little stimulated translocation, whereas Syk-CFP very rapidly translocates to the PM in response to antigen stimulation (*upper panels* in Fig. 6, *B* and *C*). The GFP-(Akt)-PH that is PM-associated exhibits a relatively high degree of colocalization with crosslinked receptors and CTB. As summarized in Table 1, the average ρ_0 values for this probe are comparable to those seen for GFP-(PLC-γ1)-$(SH2)_2$, and persist over the 20-min time period of observation (Fig. 6 *C*, *lower panel*). In contrast, Syk-CFP, despite its rapid PM translocation, exhibits very limited receptor colocalization, with ρ_0 values near 0 (Fig. 6 *D*, *lower panel*). The ρ_0 values for Syk-CFP and CTB are somewhat greater than those for Syk-CFP and antigen, and they exhibit only a small, slow increase after antigen addition, suggesting that the recruited Syk-CFP may be localized to a nonraft environment.

The protein serine-threonine kinase, Akt, is a downstream mediator of phosphatidylinositol 3-kinase (PI3K) activation and supplies anti-apoptotic signals that are critical for cell survival and proliferation (23). PI3K is activated after receptor crosslinking and phosphorylates phosphatidylinositol-4,5-bisphosphate (PIP_2) at the D3 position of the inositol ring to produce phosphatidylinositol-3,4,5-trisphosphate (PIP_3), an important lipid second messenger at the PM (24). Multiple signaling proteins, including Akt and Bruton's tyrosine kinase, bind to PIP_3 via their pleckstrin-homology (PH) domains. Thus, GFP-(Akt)-PH provides a useful means of directly observing the spatial localization of PIP_3 produced in activated cells (25). This fluorescent probe was previously used to demonstrate rapid PIP_3 production within minutes of the formation of an immunological synapse between a T cell and an antigen-presenting cell, and a persistent PIP_3 concentration at the synapse over long times (26,27). Our quantitative analysis also shows a small time-dependent increase in the PM accumulation of this probe, and a relatively high degree of association with crosslinked receptor, and with CTB (Fig. 6 *B*), suggesting a constitutive presence of PIP_3 at the PM moderately colocalizing with crosslinked IgE receptors.

Syk is a member of the Syk/ZAP-70 family whose structure consists of an N-terminal domain with tandem SH2, connected via a linker region to a C-terminal kinase domain. The tandem SH2 domain of Syk specifically targets the phosphorylated ITAMs of the γ-subunits of FcεRI (28). Using RBL cells transfected with a GFP-labeled N-terminal domain of Syk, Stauffer and Meyer (7) demonstrated that it is rapidly recruited to the PM after IgE receptor stimulation. Our study examined holo Syk with CFP conjugated to its carboxy-terminus. The sequence of confocal images in Data S1, Fig. S3 shows the PM distribution of Syk-CFP and Cy5-DNP-BSA in a typical experiment. Within 30 s after antigen addition, and preceding the formation of detectable receptor clustering, there is a visually detectable enhancement in Syk-CFP fluorescence at the PM. Quantitative analysis of the PM intensity in this channel (Fig. 6 *D*, *upper panel*) also confirms this visual impression. Thus, the recruitment of the holoenzyme to the PM, mediated via the tandem SH2, is similar to that of the previously characterized N-terminal domain alone (7). The PM recruitment of Syk-CFP that we observe is consistent with its rapid activation to an open conformation: In its unbound state Syk is autoinhibited by a conformational association of the kinase domain with the tandem SH2, such that neither can interact with binding partners. Binding of the tandem SH2 to phosphorylated ITAMs on FcεRI relieves this inhibition and leads to an open and more active conformation of the enzyme (29). The kinase activity is further enhanced by an autophosphorylation at the regulatory loop of the kinase domain (30).

The lack of colocalization of Syk-CFP with receptor clusters (*lower panel* in Fig. 6 *C* and Data S1, Fig. S3) suggests the presence of other PM targets for this kinase. Possible candidates include integrin-associated ITAM-containing DAP12 (31), and phospholipase D2 (32). Alternatively, the

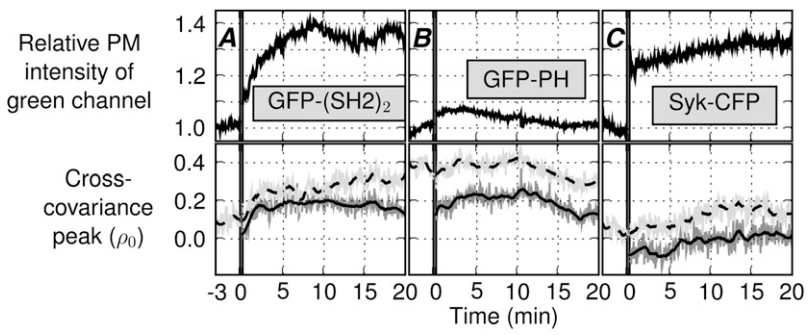

FIGURE 6 Dynamics of PM recruitment and colocalization with crosslinked receptor and CTB for (*A*) GFP-(PLC-γ1)-$(SH2)_2$, (*B*) GFP-(Akt)-PH, and (*C*) Syk-CFP. Each plot shows the average of data from 8 to 16 individual cells acquired in 4–8 independent experiments on different days. The top panels plot a normalized mean intensity at the PM in the green channel. The intensity values from each experiment were first normalized with respect to the average of the intensity values before antigen addition (i.e., the average of the first 61 frames), and these normalized data for all the experiments were averaged for the plots shown here. The bottom panels show the peak cross-covariance ρ_0 (Eq. 6) between the PM distributions of each protein and crosslinked receptor (*solid trace* on *shading*), and CTB (*dashed trace* on *light shading*), averaged for all the experiments. The smooth lines through the cross-covariance data were generated as described in Fig. 5.

TABLE 1 Summary of peak cross-covariance (ρ_0) values and their relative measure of coincidence

Fluorophore pair	Mean ρ_0*	% Max. overlap
Cytosolic probes		
Syk-CFP × Cy5-DNP-BSA	−0.031 ± 0.003	0
ECFP-InsP51 × A647-DNP-BSA	0.142 ± 0.005	24.8 ± 5.1
GFP-(PLC-γ1)-$(SH2)_2$ × Cy5-DNP-BSA	0.171 ± 0.002	28.9 ± 4.7
GFP-(PLC-γ1)-$(SH2)_2$ × A555-CTB (pre-antigen)	0.0978 ± 0.005	18.4 ± 5.15
GFP-(PLC-γ1)-$(SH2)_2$ × A555-CTB (post-antigen)	0.270 ± 0.003	43.1 ± 4.8
GFP-(Akt)-PH × Cy5-DNP-BSA	0.200 ± 0.002	33.0 ± 4.7
Membrane-associated probes		
GFP-Cdc42-N17 × A647-DNP-BSA	0.157 ± 0.004	26.8 ± 4.9
LynB-EGFP × Cy5-DNP-BSA	0.283 ± 0.002	44.9 ± 4.6
PM-EGFP × Cy5DNP-BSA	0.263 ± 0.003	42.0 ± 4.7
LAT-EGFP × Cy5-DNP-BSA	0.318 ± 0.002	49.8 ± 4.7
A488-IgE × Cy5-DNP-BSA	0.669 ± 0.003	100

The ρ_0 values are scaled between the minimum observed overlap between Syk-CFP and Cy5-DNP-BSA and the maximum observed overlap between A488-IgE and Cy5-DNP-BSA.

*The data are presented as mean ± standard error. The mean was calculated by averaging the observed ρ_0 values over all time points, for 8–16 individual cells for each fluorophore pair.

low observed ρ_0 between Syk-CFP and crosslinked receptors could be the result of chromatic aberration arising from a poor correction of microscope optics at the shorter wavelengths used for imaging CFP. To determine whether these unusually low ρ_0 values are caused by such an optical artifact of using a CFP label, we also examined the cross-covariance of ECFP-labeled inositol phosphate 5-phosphatase (ECFP-InsP51) (14) with crosslinked receptors. This chimeric protein is partially localized to the PM, and partially cytosolic, and this distribution is unchanged upon antigen binding (data not shown). The time course of ρ_0 between ECFP-InsP51 and crosslinked receptor is plotted in Data S1, Fig. S4, and shows a robust stimulated increase within 3–5 min after antigen addition, synchronous with the time course of antigen binding in these experiments. After antigen binding, ρ_0 values observed are similar to those between GFP-(PLC-γ1)-$(SH2)_2$ and crosslinked receptors, indicating a similar degree of colocalization (Table 1). Thus, it is unlikely that the low values of ρ_0 between Syk-CFP and crosslinked receptor that we observe are an optical artifact of the CFP reporter.

In previous studies, Wilson et al. (33,34) used high-resolution transmission electron microscopy to observe membrane sheets isolated from fixed RBL-2H3 cells. These authors reported a marked colocalization between immunogold-labeled Syk and FcεRI, in osmiophilic patches, after receptor crosslinking at 37°C. In our experiments, we do not detect cross-covariance between Syk-CFP and receptor-bound Cy5-antigen, and there are several possibilities for the lack of consistency between our results and those of Wilson et al. (33,34). In our experimental system, Syk-CFP competes with endogenous Syk for ITAM binding, and the detection of the fluorescently-labeled fraction may be limited by an excess of endogenous Syk. To assess whether the lack of observed colocalization of Syk-CFP is due to the presence of endogenous unlabeled Syk, we used immunofluorescent labeling to examine the distribution of endogenous Syk in response to antigen stimulation.

Data S1, Fig. S5 shows representative images of mast cells sensitized with A488-IgE, unstimulated (*top panel*), or incubated with DNP-BSA for 2 min (*middle panel*) or 5 min (*bottom panel*) at 37°C. The corresponding images of Syk, immunolabeled with the N-19 anti-Syk antibody, are shown in the second column. In unstimulated cells, A488-IgE is distributed uniformly at the PM and endogenous Syk is relatively uniformly distributed with very limited localization at the PM. Within 2 min of antigen stimulation, A488-IgE is dramatically redistributed into distinct membrane punctae. In contrast, Syk shows a relatively uniform increase at the PM (*arrows*, *middle panel*), and no patchiness or colocalization with the IgE punctae. After 5 min of antigen stimulation, endogenous Syk clearly redistributes into dorsal membrane ruffles (*bottom panel*), and is well segregated from IgE patches that do not localize in ruffles. The distinct and non-overlapping distributions of IgE and endogenous Syk, observed in these images of fixed cells, is consistent with our analysis of real-time confocal images of Syk-CFP described above.

Our results suggest that Syk is only transiently associated with crosslinked, phosphorylated FcεRI in these cells during its ITAM-dependent activation, such that other proteins, both PM-associated and cytoplasmic, can compete with FcεRI for Syk once it is activated. In B-cells, the majority of activated Syk is localized to the cytosolic fraction, and the phosphorylation of Tyr-130 on Syk appears to mediate its dissociation from crosslinked B-cell receptors (35,36). Interestingly, in a recent study, Ilani et al. showed that the localization of Syk family member Zap70 in T cells to immune synapses is mediated by direct interaction of activated Zap70 with the cytoskeletal protein Ezrin (Illani, T., C. Khanna, M. Zhou, T. D. Veenstra, and A. Bretscher. 2007. Immune synapse formation requires ZAP-70 recruitment by ezrin and CD43 removal by moesin. *J. Cell Biol.* In press). Further studies on the EM distributions of Syk in conventionally fixed and permeabilized cells may help to address the apparent discrepancy between the fluorescence imaging results described here and the EM results on pulled-away membrane patches described previously (33).

Colocalization dynamics of membrane-associated signaling components

We also examined the dynamics of several PM-associated proteins, including protein tyrosine kinase Lyn (Lyn-EGFP) anchored to the inner PM leaflet (11,37) and the transmembrane adaptor protein LAT (LAT-EGFP). LAT and Lyn

contain dual palmitate and palmitate-myristate acylations, respectively, that localize these proteins to lipid rafts (8,38). Consistent with their substantial lipid raft association, we observe a high level of basal colocalization with CTB, with basal ρ_0 values $\gtrsim$0.4 for both of these proteins. After antigen stimulation, the degree of colocalization with crosslinked receptor and CTB steadily increases during the first ~5–10 min (Fig. 7, *A* and *B*), consistent with the lipid raft association of crosslinked receptor (39). We also observe a rapid ~20% increase in the LAT-EGFP intensity at the PM after antigen addition, followed by a slow, time-dependent decline, suggesting stimulated trafficking of an intracellular membrane compartment containing additional LAT. A similar process has been described in activated T-cells (40).

The inner leaflet marker PM-EGFP contains the minimal Lyn sequence necessary for its membrane anchorage via dual myristoyl and palmitoyl acylations (8), and exhibits similar mean ρ_0 values as Lyn, but greater temporal variability, and

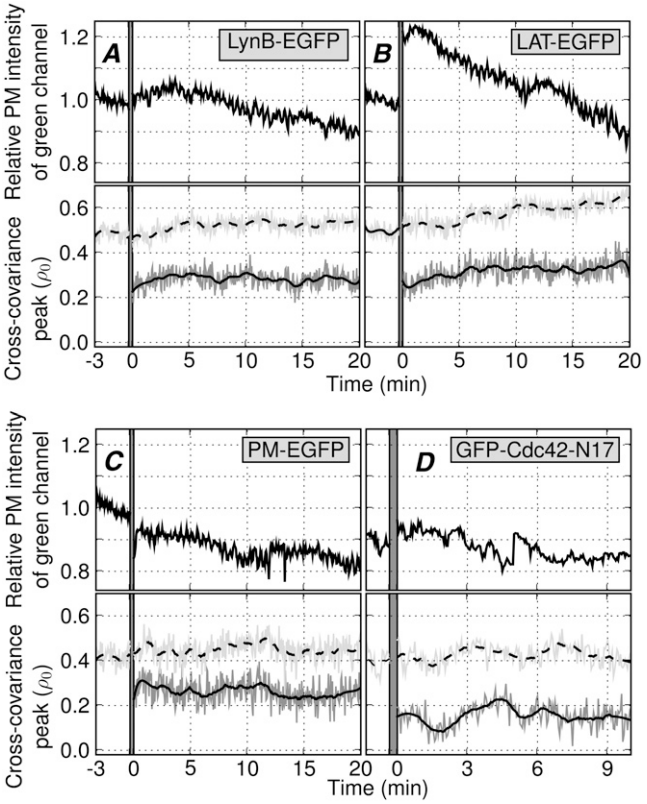

FIGURE 7 Dynamics of co-redistribution with crosslinked receptor for the predominantly PM-associated proteins (*A*) LynB-EGFP, (*B*) PM-EGFP, (*C*) LAT-EGFP, and (*D*) EGFP-Cdc42-N17. Each plot shows the average of data for 5–10 individual cells from two-to-five independent experiments on different days for each fluorescent chimera. The top panel plots the mean intensity at the PM in the green channel, normalized to the average of the preantigen intensity for each experiment and corrected for photobleaching. The bottom panel shows the peak cross-covariance ρ_0 (Eq. 6) between the PM distributions of each protein and crosslinked receptor (*solid trace* on *shading*), and CTB (*dashed trace* on *light shading*), averaged for all the experiments. The smooth curves through the cross-covariance data were generated as described in Fig. 5.

no net increase in colocalization due to stimulation by antigen (Fig. 7 *C*). A previous study using ligand-containing patterned lipid bilayers to stimulate RBL-2H3 cells at 37°C detected Lyn-EGFP accumulation at the patterns after ~15 min of stimulation, and accumulation of PM-EGFP followed an even slower time course (41). The more rapid kinetics we observe for increases in receptor colocalization of Lyn-EGFP and LAT-EGFP could arise from differences between stimulation due to soluble antigen versus patterned bilayers. In particular, significant accumulation of labeled proteins at sites of crosslinked receptors on micron-sized patterned bilayer patches require two-dimensional diffusion on a larger length-scale, and the kinetics of this level of accumulation may limit the detection of this colocalization at shorter stimulation times. In contrast, the kinetics of diffusion on the smaller length scale, necessary for detectable colocalization in our experiments, are likely to be faster, resulting in a commensurately shorter timescale for the detection of a change in colocalization.

We note that ρ_0 values for these membrane-anchored components are generally somewhat higher than the ρ_0 values observed for cytosolic probes that colocalize with the crosslinked receptor (Table 1). The reason for these generally higher ρ_0 values is unknown, but one possibility is that the finite width of the PM mask generated in our analysis captures both PM-associated as well as cytosolic fractions of cytosolic proteins. Because the cytosolic fraction is generally uniformly distributed, it diminishes the contributions to ρ_0 from the PM-associated fraction. Thus, for cytosolic proteins, ρ_0 likely underestimates the degree of receptor colocalization. In contrast, for proteins that are predominantly PM-associated, there is no such attenuating contribution from the cytosol, resulting in the higher ρ_0 values.

It is also possible that the higher ρ_0 values arise from a greater lateral proximity between proteins that partition favorably into liquid-ordered lipid raft domains. Unlike, Lyn and LAT, the Rho-family GTPase Cdc42 is anchored to the PM by basic amino acids and geranyl-geranyl acylation, and, as previously reported, exhibits very limited colocalization with crosslinked IgE receptors in lipid rafts (8,21). To compare the effect of these different membrane anchors, we examined the colocalization dynamics of GFP-Cdc42-N17, a GFP-labeled, noncatalytic mutant of Cdc42 (15). This protein partially localizes to the plasma membrane (data not shown), and this association is not significantly altered after antigen stimulation (Fig. 7 *D*). Consistent with results from previous studies on endogenous Cdc42 (8,21), GFP-Cdc42-N17 exhibits a substantially lower receptor colocalization compared to other PM-associated proteins, with ρ_0 values $\lesssim$0.2 (Table 1). These differences are further illustrated in Fig. 8 where we compare histograms of ρ_0 values for EGFP-Lyn and GFP-Cdc42-N17. The relatively lower ρ_0 values for this protein compared to the lipid raft-associated Lyn and LAT indicate that in our experimental system, lipid order-mediated partitioning of membrane-associated proteins

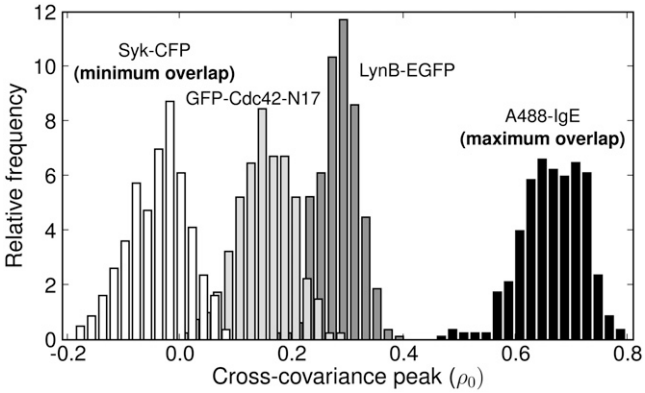

FIGURE 8 Distribution of peak cross-covariance (ρ_0) values for the membrane-associated probes EGFP-Cdc42-N17 and Lyn-EGFP. Also shown for reference are the distributions of peak cross-covariance data for the two limiting cases of complete overlap (between Cy5-DNP-BSA and A488-IgE, Fig. 5) and no overlap (between Syk-CFP and Cy5-DNP-BSA, Fig. 6).

influences their observed cross-covariance with crosslinked IgE receptors.

SUMMARY

We developed an automated image analysis scheme that significantly expands the applicability of a cross-covariance analysis to quantify colocalization between PM-associated signaling components. We used time-lapse confocal fluorescence microscopy to image living RBL-2H3 mast cells at physiologically relevant temperatures, with a time resolution of 3 s/frame, before and during stimulation by a multivalent antigen. We used a fluorescently-labeled antigen (Cy5-DNP-BSA) to visualize the crosslinked receptor, and transiently transfected fluorescent fusion proteins to visualize specific signaling components. The PM was labeled by a brief incubation with A555-CTB. Our image analysis utilizes the CTB label image to extract a binary PM mask, and uses this mask to obtain the PM distribution of crosslinked receptors and fluorescent chimera. It then calculates the mean intensity of the fluorescent protein conjugates as a measure of its translocation to the PM, and the peak cross-covariance (ρ_0) between the two PM distributions as a measure of their relative overlap. The image analysis tools we developed can rapidly analyze hundreds of images to obtain a statistically meaningful description of these quantitative measures of translocation and colocalization in real time.

The ρ_0 value for two labeled species measures a correlated overlap in deviations about the respective means of the spatial distributions for the two species. Thus, ρ_0 effectively measures how well two distributions are correlated independent of any changes in their mean values alone. It is therefore a useful metric for quantifying the colocalization between two fluorophores even when their overall intensities change relative to each other, as is the case when a cytosolic probe translocates to the membrane in response to antigen crosslinking. A previous study in our laboratory (8) used a series of simulated intensity distributions to develop a theoretical framework for applying a cross-covariance analysis to confocal microscopy images and interpreting the cross-covariance data. One important conclusion of this study was that spurious cross-correlations observed due to membrane morphology alone are essentially eliminated with the inclusion of noise. Thus, for the signal/noise ratio typical in our experiments, ρ_0 is also minimally influenced by the overall cell shape and membrane morphology. In this and other studies, plasma membrane traces were generated manually from confocal images of cells under consideration, and cross-covariance between the two fluorophore distributions along these manual traces was then calculated. The technique for calculating cross-covariance that we present here measures essentially the same physical quantity as those previously reported (7,8) but adopts a somewhat different strategy with particular advantages.

The most significant advance that our scheme offers is the use of the segmentation algorithm to generate a PM mask in an automated fashion, therefore eliminating the need to draw a manual PM trace by hand. This automated PM definition greatly expands the applicability of the cross-covariance measurement by allowing a rapid analysis of stacks of multiple images. In a typical experiment we generate $\gtrsim$400 image frames in $\sim$20 min of image acquisition. Because of small drifts in the stage position and subtle to profound changes in cell morphology, the definition of the PM alters in the course of an experiment. Therefore, generating an accurate trace of the PM by hand for all the images in an experiment is quite laborious and impractical. Consequently, cross-covariance measurements between membrane-associated components has in the past been limited to the analysis of a comparatively small number of images, frequently of fixed cells, and at intervals of 1 min or longer after receptor crosslinking. In contrast, we are able to efficiently analyze multiple experiments and generate a much more detailed quantitative picture of the dynamics of translocation and receptor colocalization. When compounded with averages over multiple independent experiments, this automated analysis can generate data with a high statistical significance. Thus, for example, the plot shown in Fig. 5 *A* is a composite of this image analysis applied to $>$6400 individual confocal snapshots.

We applied this image acquisition and analysis to a set of cytosolic and membrane associated signaling components and determined the dynamics of translocation of the cytosolic probes to the PM, and colocalization of these and other membrane-associated components with crosslinked IgE receptors and CTB. Our analysis reveals facets of FcϵRI-mediated signaling in RBL cells that are difficult to determine from simple visualization of confocal microscopy images. The histograms in Fig. 5 *G* and Fig. 8 reveal the level of statistical detail that is attainable using our analysis, such that

small differences in the relative colocalization of different signaling proteins can be distinguished. We found evidence for a biphasic PM recruitment pattern of the tandem SH2 domain of PLC-γ1 during the time period of observation. We also found a high degree of colocalization between crosslinked IgE receptors and the PM-associated PIP_3-specific PH domain from Akt and crosslinked IgE receptors, suggesting a constitutive presence of PIP_3 at the PM that associates with crosslinked receptors.

Both LynB-EGFP and LAT-EGFP exhibit time-dependent increases in receptor colocalization after antigen stimulation that are consistent with the formation of tyrosine phosphorylation-driven signaling complexes (42). A comparable degree of receptor colocalization for the lipid-raft-associated inner leaflet marker PM-EGFP, and lower ρ_0 values for the non-raft-associated GFP-Cdc42-N17, together suggest that the interactions observed under these conditions at the resolution of confocal imaging are also influenced by lipid order-dependent membrane organization. In contrast, there is little or no detectable colocalization of Syk-CFP with crosslinked receptors even though it undergoes a rapid and substantial PM translocation after antigen stimulation. This result points to a transient interaction between activated Syk and the receptor complex, that might arise from the dissociation of phosphorylated Syk from crosslinked receptor, and its interaction with components of other signaling pathways activated as a result of antigen crosslinking.

Recent advances in time-resolved three-dimensional imaging, so-called four-dimensional imaging (43), of biological systems have made it feasible to acquire detailed spatio-temporal data for subcellular localization of signaling proteins. The image analysis tools described here are broadly applicable, and we expect it will be straightforward to adapt this analysis scheme for analyzing such data for other cells.

SUPPLEMENTARY MATERIAL

To view all of the supplemental files associated with this article, visit www.biophysj.org.

We thank Carol Bayles at Cornell's Microscopy, Imaging and Fluorimetry Facility for assistance with confocal microscopy.

This work was supported by National Science Foundation-Science and Technology Center Nanobiotechnology Center at Cornell (grant No. ECS-9876771) and by National Institutes of Health grant No. AI 22449.

REFERENCES

1. Kawakami, T., and S. Galli. 2002. Regulation of mast-cell and basophil function and survival by IgE. *Nat. Rev. Immunol.* 2:773–786.
2. Kinet, J. 1999. The high-affinity IgE receptor (FcεRI): from physiology to pathology. *Annu. Rev. Immunol.* 17:931–972.
3. Kimura, T., H. Sakamoto, E. Appella, and R. Siraganian. 1996. Conformational changes induced in the protein tyrosine kinase p72syk by tyrosine phosphorylation or by binding of phosphorylated immunoreceptor tyrosine-based activation motif peptides. *Mol. Cell. Biol.* 16:1471–1478.
4. El-Hillal, O., T. Kurosaki, H. Yamamura, J. Kinet, and A. Scharenberg. 1997. Syk kinase activation by a Src kinase-initiated activation loop phosphorylation chain reaction. *Proc. Natl. Acad. Sci. USA.* 94:1919–1924.
5. Miyawaki, A., A. Sawano, and T. Kogure. 2003. Lighting up cells: labeling proteins with fluorophores. *Nat. Cell Biol.* 5:S1–S7.
6. Holowka, D., J. Gosse, A. Hammond, X. Han, P. Sengupta, N. Smith, A. Wagenknecht-Wiesner, M. Wu, R. Young, and B. Baird. 2005. Lipid segregation and IgE receptor signaling: a decade of progress. *Biochim. Biophys. Acta.* 1746:252–259.
7. Stauffer, T., and T. Meyer. 1997. Compartmentalized IgE receptor-mediated signal transduction in living cells. *J. Cell Biol.* 139:1447–1454.
8. Pyenta, P., D. Holowka, and B. Baird. 2001. Cross-correlation analysis of inner-leaflet-anchored green fluorescent protein co-redistributed with IgE receptors and outer leaflet lipid raft components. *Biophys. J.* 80:2120–2132.
9. Liu, F., J. Bohn, E. Ferry, H. Yamamoto, C. Molinaro, L. Sherman, N. Klinman, and D. Katz. 1980. Monoclonal dinitrophenyl-specific murine IgE antibody: preparation, isolation, and characterization. *J. Immunol.* 124:2728–2737.
10. Posner, R., B. Lee, D. Conrad, D. Holowka, B. Baird, and B. Goldstein. 1992. Aggregation of IgE-receptor complexes on rat basophilic leukemia cells does not change the intrinsic affinity but can alter the kinetics of the ligand-IgE interaction. *Biochemistry.* 31:5350–5356.
11. Larson, D., J. Gosse, D. Holowka, B. Baird, and W. Webb. 2005. Temporally resolved interactions between antigen-stimulated IgE receptors and Lyn kinase on living cells. *J. Cell Biol.* 171:527–536.
12. Servant, G., O. D. Weiner, P. Herzmark, T. Balla, J. W. Sedat, and H. R. Bourne. 2000. Polarization of chemoattractant receptor signaling during neutrophil chemotaxis. *Science.* 287:1037–1040.
13. Bunnell, S. C., V. Kapoor, R. P. Trible, W. Zhang, and L. E. Samelson. 2001. Dynamic actin polymerization drives T cell receptor-induced spreading: a role for the signal transduction adaptor LAT. *Immunity.* 14:315–329.
14. Stolz, L. E., W. J. Kuo, J. Longchamps, M. K. Sekhon, and J. D. York. 1998. INP51, a yeast inositol polyphosphate 5-phosphatase required for phosphatidylinositol 4,5-bisphosphate homeostasis and whose absence confers a cold-resistant phenotype. *J. Biol. Chem.* 273:11852–11861.
15. Michaelson, D., J. Silletti, G. Murphy, P. D'Eustachio, M. Rush, and M. R. Philips. 2001. Differential localization of ρ-GTPases in live cells: regulation by hypervariable regions and ρGDI binding. *J. Cell Biol.* 152:111–126.
16. Barsumian, E., C. Isersky, M. Petrino, and R. Siraganian. 1981. IgE-induced histamine release from rat basophilic leukemia cell lines: isolation of releasing and nonreleasing clones. *Eur. J. Immunol.* 11:317–323.
17. Pierini, L., D. Holowka, and B. Baird. 1996. FcεRI-mediated association of 6-micron beads with RBL-2H3 mast cells results in exclusion of signaling proteins from the forming phagosome and abrogation of normal downstream signaling. *J. Cell Biol.* 134:1427–1439.
18. Otsu, N. 1979. A threshold selection method from gray-level histograms. *IEEE T. Syst. Man. Cyb.* 9:62–66.
19. Kreyszig, E. 2002. Advanced Engineering Mathematics. John Wiley & Sons, New York.
20. Lencer, W., T. Hirst, and R. Holmes. 1999. Membrane traffic and the cellular uptake of cholera toxin. *Biochim. Biophys. Acta.* 1450:177–190.
21. Holowka, D., E. D. Sheets, and B. Baird. 2000. Interactions between FcεRI and lipid raft components are regulated by the actin cytoskeleton. *J. Cell Sci.* 113:1009–1019.
22. Haugh, J., F. Codazzi, M. Teruel, and T. Meyer. 2000. Spatial sensing in fibroblasts mediated by 3′ phosphoinositides. *J. Cell Biol.* 151:1269–1280.
23. Coffer, P., J. Jin, and J. Woodgett. 1998. Protein kinase B (c-Akt): a multifunctional mediator of phosphatidylinositol 3-kinase activation. *Biochem. J.* 335:1–13.

24. Fruman, D., and L. Cantley. 2002. Phosphoinositide 3-kinase in immunological systems. *Semin. Immunol.* 14:7–18.

25. Halet, G. 2005. Imaging phosphoinositide dynamics using GFP-tagged protein domains. *Biol. Cell.* 97:501–518.

26. Harriague, J., and G. Bismuth. 2002. Imaging antigen-induced PI3K activation in T cells. *Nat. Immunol.* 3:1090–1096.

27. Costello, P., M. Gallagher, and D. Cantrell. 2002. Sustained and dynamic inositol lipid metabolism inside and outside the immunological synapse. *Nat. Immunol.* 3:1082–1089.

28. Kihara, H., and R. Siraganian. 1994. Src homology 2 domains of Syk and Lyn bind to tyrosine-phosphorylated subunits of the high affinity IgE receptor. *J. Biol. Chem.* 269:22427–22432.

29. Siraganian, R., J. Zhang, K. Suzuki, and K. Sada. 2002. Protein tyrosine kinase Syk in mast cell signaling. *Mol. Immunol.* 38:1229–1233.

30. Reth, M., and T. Brummer. 2004. Feedback regulation of lymphocyte signaling. *Nat. Rev. Immunol.* 4:269–277.

31. Lanier, L. L. 2005. NK cell recognition. *Annu. Rev. Immunol.* 23:225–274.

32. Lee, J. H., Y. M. Kim, N. W. Kim, J. W. Kim, E. Her, B. K. Kim, J. H. Kim, S. H. Ryu, J. W. Park, D. W. Seo, J. W. Han, M. A. Beaven, and W. S. Choi. 2006. Phospholipase D2 acts as an essential adaptor protein in the activation of Syk in antigen-stimulated mast cells. *Blood.* 108:956–964.

33. Wilson, B., J. Pfeiffer, and J. Oliver. 2000. Observing FcεRI signaling from the inside of the mast cell membrane. *J. Cell Biol.* 149:1131–1142.

34. Wilson, B., J. Pfeiffer, Z. Surviladze, E. Gaudet, and J. Oliver. 2001. High resolution mapping of mast cell membranes reveals primary and secondary domains of FcεRI and LAT. *J. Cell Biol.* 154:645–658.

35. Peters, J. D., M. T. Furlong, D. J. Asai, M. L. Harrison, and R. L. Geahlen. 1996. Syk, activated by crosslinking the B-cell antigen receptor, localizes to the cytosol where it interacts with and phosphorylates α-tubulin on tyrosine. *J. Biol. Chem.* 271:4755–4762.

36. Keshvara, L. M., C. Isaacson, M. L. Harrison, and R. L. Geahlen. 1997. Syk activation and dissociation from the B-cell antigen receptor is mediated by phosphorylation of tyrosine 130. *J. Biol. Chem.* 272: 10377–10381.

37. Hess, S., E. Sheets, A. Wagenknecht-Wiesner, and A. Heikal. 2003. Quantitative analysis of the fluorescence properties of intrinsically fluorescent proteins in living cells. *Biophys. J.* 85:2566–2580.

38. Zhang, W., R. Trible, and L. Samelson. 1998. LAT palmitoylation: its essential role in membrane microdomain targeting and tyrosine phosphorylation during T cell activation. *Immunity.* 9:239–246.

39. Field, K., D. Holowka, and B. Baird. 1997. Compartmentalized activation of the high affinity immunoglobulin E receptor within membrane domains. *J. Biol. Chem.* 272:4276–4280.

40. Bonello, G., N. Blanchard, M. C. Montoya, E. Aguado, C. Langlet, H. T. He, S. Nunez-Cruz, M. Malissen, F. Sanchez-Madrid, D. Olive, C. Hivroz, and Y. Collette. 2004. Dynamic recruitment of the adaptor protein LAT: LAT exists in two distinct intracellular pools and controls its own recruitment. *J. Cell Sci.* 117:1009–1016.

41. Wu, M., D. Holowka, H. Craighead, and B. Baird. 2004. Visualization of plasma membrane compartmentalization with patterned lipid bilayers. *Proc. Natl. Acad. Sci. USA.* 101:13798–13803.

42. Silverman, M. A., J. Shoag, J. Wu, and G. A. Koretzky. 2006. Disruption of SLP-76 interaction with GADS inhibits dynamic clustering of SLP-76 and FcεRI signaling in mast cells. *Mol. Cell. Biol.* 26:1826–1838.

43. Gerlich, D., and J. Ellenberg. 2003. 4D imaging to assay complex dynamics in live specimens. *Nat. Cell Biol.* 5:S14–S19.

44. Press, W. H., S. A. Teukolsky, W. T. Vellerling, and B. P. Flannery. 1992. Numerical Recipes in C, 2nd Ed. Cambridge University Press, Cambridge, UK.